complexes when $|A^{Cu}|$ is nearly equal to $|A^{Br}|$ ($|A^{Br}/A^{Cu}| \approx 1$), which corresponds to the cases of $[Cu(NS_3)Br]^+$ and $[Cu(N_2S_2B)Br]^+$.

When $|A^{Br}/A^{Cu}|$ is not equal to 1, the observable spectrum will depend on the ratio $|A^{Br}/A^{Cu}|$ and the line width of the peak. On the basis of the frozen ESR spectrum (77 K), it is clear that $[Cu(NS_2)Br]^+$ has a square-planar structure

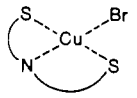

and it is less likely that there is an equilibrium of the trigonal bipyramid and the square pyramid in solution, because NS_2 is not a tripodlike ligand. Thus, it seems most reasonable to assume that the $|A^{Br}/A^{Cu}|$ value in this complex is not equal to 1, although the exact $|A^{Br}/A^{Cu}|$ value cannot be evaluated at present. If two or three peaks in the higher field of $[Cu(NS_2)Br]^+$ collapse to one broad band, such a spectrum should resemble those of $[Cu(N_2S_2P)Br]^+$, $[Cu(N_3S)Br]^+$, etc. Thus, we can elucidate the solution ESR spectra of X = Br^- complexes in terms of the scheme in Figure 10 on the assumption that the ratio $|A^{Br}/A^{Cu}|$ is variable due to the change of the ligand character.

The same discussion as described above is also applicable to the X = I^- complexes: If $|A^I| = |A^{Cu}|$, nine hyperfine lines are expected, which is verified by the $[Cu(NS_3)I]^+$ and $[Cu(N_2S_2P)I]^+$ complexes. If $|A^I/A^{Cu}| \neq 1$, the observable hyperfine lines should change, and this is confirmed by several examples; seven lines are observed for $[Cu(N_4P)I]^+$, and a very complicated spectrum was observed for $[Cu(N_3S)I]^+$ in nitromethane. Thus, we can successfully elucidate the unusual solution ESR spectra observed in this study on the assumption that the unpaired electron of the copper(II) ion interacts with the nuclear spins of both copper and halogen atoms, and its ratio $|A^X/A^{Cu}|$ is variable, depending on the ligand used.

In the case where the metal ion has a single open-shell orbital, φ, occupied with, e.g., spin α (denoted by φ^+) and the neighboring closed-shell ion (halogen ion in the present case) has an occupied pair of orbitals, χ^+ and χ^-, with the same spatial symmetry as φ, these orbitals will in general not be orthogonal but will have an overlap integral $S \neq 0$ between them. Thus the total wave function for a three-electron system is, to zero order, given by $|\chi^+{}_b\chi^-{}_b\varphi^+{}_b|$, where

$$\chi_b = 1/N_a^{1/2}(\chi + \gamma\varphi)$$

$$\varphi_b = 1/N_b^{1/2}(\varphi - \lambda\chi)$$

and γ is called a "covalent" mixing factor.[31,32] If we assume $N_a \approx N_b \approx 1$, we get[33] $\lambda = (\gamma + S)/(1 + \gamma S) \approx \gamma + S$. These "overlap" and "covalent" effects convey a spin density onto ligand sites whose spin direction is parallel to that of the local metal moment. This is the main origin for the nonzero value of A^X.[31,32] The unpaired spin density on the halogen atom is roughly calculated to be $\lambda^2/2N_a$;[33] this indicates that the A^X increases when the energy gap between φ(d orbital) and χ(halogen atom) decreases.[34] Thus, we can estimate that γ is variable due to the change of ligand atoms, because the energy of the d orbital is dependent on the ligand atoms surrounding the metal ion as exemplified by the fact that the reduction potential of [Cu(L)X]Y is highly dependent on the ligand character.[12] The above discussion supports our assumption that the ratio $|A^X/A^{Cu}|$ is variable due to the change of the ligand.

Registry No. **1**, 113321-86-1; **2**, 113321-88-3; **3**, 113321-90-7.

Supplementary Material Available: Listings of details of the experimental conditions in the X-ray data collection, atomic coordinates, anisotropic temperature factors, and all bond distances and angles (10 pages); complete listings of F_o and F_c values (43 pages). Ordering information is given on any current masthead page.

(31) Watson, R. E.; Freeman, A. J. In *Hyperfine Interaction*; Freeman, A. J., Frankel, R. B., Eds.; Academic: New York, 1967; Chapter 2.
(32) Abragam, A.; Bleaney, B. *Electron Paramagnetic Resonance of Transition Ions*; Clarendon: Oxford, England, 1970; Chapter 17.
(33) Kamimura, H.; Sugano, S.; Tanabe, Y. *Ligand Field Theory and Its Applications*; Shokabo: Tokyo, 1970; Chapter 12 (in Japanese).
(34) Jørgensen, C. K. *Modern Aspects of Ligand Field Theory*; North-Holland: Amsterdam, 1971.

Contribution from the Departments of Chemistry, University of Florida, Gainesville, Florida 32611, and University of New Orleans, New Orleans, Louisiana 70148

Coordination Chemistry, Inductive Metal-Metal Bond Transfer, and Magnetic Susceptibility of Adducts of Tetrakis(trifluoroacetato)dichromium

Carl J. Bilgrien,[†] Russell S. Drago,*[†] Charles J. O'Connor,*[‡] and Ngai Wong

Received November 20, 1987

Bonding of donors (B) to chromium(II) trifluoromethanecarboxylates, $Cr_2(O_2CCF_3)_4$, has been explored with respect to the influence one Cr-L bond has on the other. In order to obtain enthalpies for the free acid, a displacement reaction had to be studied, and a novel extension of the *E*, *C*, and W equation was derived to provide this information. Despite the weak chromium-chromium bond, adduct formation at one axial site is found to significantly lower the enthalpy of adduct formation at the second. Enthalpies and equilibrium constants for first and second adduct formation with a range of donors were measured and the data used to calculate transmittance parameters by using a previously proposed inductive-transfer model in these weakly bonded metal-metal carboxylates. The $Cr_2(O_2CCF_3)_4$ core interacts with Lewis bases in primarily an electrostatic fashion, and the weak metal-metal bond was found less capable of transmitting both covalent and electrostatic effects than the metal-metal bonds in either $Mo_2(O_2CCF_2CF_2CF_3)_4$ or $Rh_2(O_2CCH_2CH_2CH_3)_4$. This is consistent with a weak covalent bond and a large Cr-Cr distance for the *C* and *E* perturbation, respectively. Magnetic susceptibility measurements of $Cr_2(O_2CCF_3)_4B_2$ adducts demonstrate a dramatic rise in the magnetic susceptibility of the adducts as the donor strength of B increases. Arguments are presented that interpret these findings as resulting from partial breaking of the metal-metal bond in proportion to donor bond strength. Consistent with this interpretation, which assumes some degree of d-orbital overlap in the $Cr_2(O_2CCF_3)_4$ core, we find singlet-triplet splittings ($-2J$ from 611 to 688 cm^{-1}) that are larger than the range observed for the extensively studied dinuclear Cu(II) carboxylates.

Introduction

The dimeric metal carboxylates, $M_2(O_2CR)_4$, are convenient systems for studying the transmission of inductive effects through the metal-metal bond of clusters. Charge neutrality allows study in noncoordinating or weakly coordinating solvents, and the metal centers display open axial (trans to the metal-metal bond) coordination sites to which Lewis bases readily bind. Earlier work from this laboratory[1-5] has focused upon spectroscopic and

[†] University of Florida.
[‡] University of New Orleans.

(1) Drago, R. S.; Tanner, S. P.; Richman, R. M.; Long, J. R. *J. Am. Chem. soc.* **1979**, *101*, 2897.
(2) Drago, R. S.; Long, J. R.; Cosmano, R. *Inorg. Chem.* **1981**, *20*, 2920.

0020-1669/88/1327-1410$01.50/0

thermodynamic studies of $Rh_2(but)_4$ (but = *n*-butyrate), $Rh_2(pfb)_4$ (pfb = perfluoro-*n*-butyrate), $Mo_2(pfb)_4$, and $Ru_2(but)_4Cl$. The rhodium and ruthenium dinuclear carboxylates, which contain π^* metal electron density, display adduct bond stabilization with σ-donor, π-acceptor Lewis bases beyond what would be expected from the simple σ-type interaction predicted with the *E* and *C* equation

$$-\Delta H + W = E_A E_B + C_A C_B \quad (1)$$

The molybdenum carboxylate, which does not contain π^* metal electron density, does not undergo these π-back-bonding interactions, and the enthalpies are well correlated with (1).

Both 1:1 and 2:1 base adducts form with the enthalpy for formation of the second metal–base bond being less than that for the first metal–base bond in the rhodium and molybdenum carboxylates. An inductive transfer model has been put forward to describe the lowering of the Lewis acidity of the second metal center.[2] The $E_A^{1:1}$ and $C_A^{1:1}$ parameters of the second center are decreased by coordination of the base in the 1:1 adduct according to

$$E_A^{1:1} = E_A - kE_B \quad (2)$$

$$C_A^{1:1} = C_A - k'C_B \quad (3)$$

The constants *k* and *k'* represent ability of the metal–metal bond to transmit the electrostatc and covalent parameters of the coordinated base. The more polarizable antibonding electron density in the single metal–metal bond of $Rh_2(but)_4$ makes this bond better able to transmit covalent effects from base coordination than the quadruple metal–metal bond of $Mo_2(pfb)_4$. On the other hand, the shorter metal–metal bond distance of $Mo_2(pfb)_4$ allows for greater electrostatic repulsion between the first base and the second base molecule.[3,5]

The analogous dinuclear chromium carboxylates are such strong Lewis acids that they are only rarely isolated without ligands coordinated to the axial acceptor sites, and then neighboring carboxylate oxygens act as donors to form an extended lattice. Coordination of an axial ligand has a pronounced effect upon the Cr–Cr distances, which range from 1.99 Å for the gas-phase $Cr_2(OAc)_4$ molecule[6] to 2.541 Å for $Cr_2(O_2CCF_3)_4(Et_2O)_2$.[7] The rhodium and molybdenum dinuclear carboxylate adducts, on the other hand, display M–M ranges of only 0.12 and 0.13 Å, respectively.[8] The Cr_2^{4+} system provides a unique opportunity to study the role an appreciably weaker Cr–Cr bond might play in the transmission of coordination effects across the metal–metal bond and to provide further tests and insights regarding (2) and (3).

An early literature report suggested that derivatives of the dinuclear chromium carboxylates exhibit weak paramagnetism.[9] The influence of the ligands upon the metal–metal bonding and the complex paramagnetism provides key information about the electronic structure of these adducts. Solid-state and solution magnetic measurements were performed on the various adducts, $Cr_2(O_2CCF_3)_4L_2$, to complement the thermodynamic studies.

Results and Discussion

An X-ray diffraction study of anhydrous $Cr_2(OAc)_4$ prepared by sublimation of the hydrate demonstrates intermolecular interactions with coordinated carboxylates on one cluster providing bridging donor oxygen atoms to acidic Cr(II) centers of a neighboring cluster.[10] To minimize the basicity of the carboxylate oxygens, the trifluoroacetate-bridged complex $Cr_2(O_2CCF_3)_4(Et_2O)_2$ (I) was utilized but a coordinating ligand (diethyl ether) is still needed to prevent aggregation and yield materials soluble in weakly polar, poorly basic solvents. Adduct formation in these studies thus proceeds via an exchange reaction to displace diethyl ether.

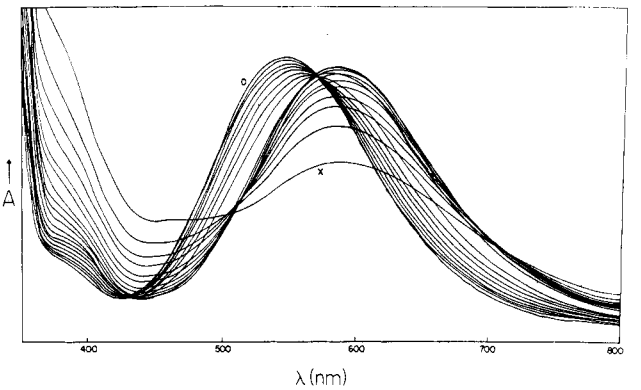

Figure 1. Spectrophotometric titration of chromium trifluoroacetate, diethyl ether adduct, with DMA in methylene chloride. The free acid (no DMA) spectrum is labeled O. The titration was ended with 50 molar excess added DMA (X).

A. Spectral Titrations. Weak donors such as acetonitrile do not displace coordinated diethyl ether. Donors of intermediate strength such as dimethylacetamide cleanly displace ether to give first a 1:1 and then a 2:1 adduct. Strong donors such as pyridine rapidly decompose the complex. For the intermediate case, equilibrium donor exchange is readily monitored by spectrophotometric titration. Representative spectra for the *N,N*-dimethylacetamide (DMA) titration of a constant amount of $Cr_2(tfa)_4(Et_2O)_2$ are shown in Figure 1. At low base concentrations the isosbestic point at 572 nm suggests two absorbing species in solution: the acid, A_2, and the 1:1 adduct, A_2B.

$$A_2 + B \overset{K_1}{\rightleftharpoons} A_2B \quad (4)$$

Further base addition results in spectral deviation from the first isosbestic point as a third species is formed in solution.

$$A_2B + B \overset{K_2}{\rightleftharpoons} A_2B_2 \quad (5)$$

The "acid A_2" refers to the bis(ether) adduct, I, and dissociation of ether accompanies coordination of B though it is not illustrated in (4) and (5).

At higher base concentration, a second isosbestic point appears at 515 nm, which upon cursory examination would appear to correspond to the conversion of A_2B to A_2B_2 (eq 5). However, quantitative analysis along with FTIR titrations reveals that the limiting spectrum centered at 585 nm corresponds to the A_2B_2 chromophore while the isosbestic point at 515 nm can be assigned to formation of yet another complex (vide infra).

$$A_2B_2 + B \rightleftarrows A_2B_3 \quad (6)$$

Though not obvious from the spectrophotometric titration, FTIR titrations show that K_1 and K_2 are large and 2 equiv of base displace both of the coordinated ethers before concentrations corresponding to the spectral changes assigned to the formation of A_2B_3 are attained. Figure 2 illustrates representative spectra for titration with DMA. The carbonyl stretch (ν_{CO}) for bound DMA is found at 1610 cm^{-1} while that for free DMA occurs at 1639 cm^{-1}. The ν_{COC} for coordinated ether occurs at 1053 cm^{-1}, while that for the free ether is at 1113 cm^{-1}. Some dissociation of diethyl ether occurs in CH_2Cl_2 solution of $Cr_2(O_2CCF_3)_4(Et_2O)_2$ even without added donor, and below 2:1 molar ratios, DMA displaces ether quite effectively. Separate shifts for coordinated DMA in the 1:1 and 2:1 DMA adduct species are not resolved.

(3) Drago, R. S.; Long, J. R.; Cosmano, R. *Inorg. Chem.* **1982**, *21*, 2196.
(4) Drago, R. S. *Inorg. Chem.* **1982**, *21*, 1697.
(5) Drago, R. S.; Cosmano, R.; Telser, J. *Inorg. Chem.* **1984**, *23*, 4514.
(6) Ketkar, S. N.; Fink, M. *J. Am. Chem. Soc.* **1985**, *107*, 338.
(7) Cotton, F. A.; Extine, M. W.; Rice, G. W. *Inorg. Chem.* **1978**, *17*, 176.
(8) Cotton, F. A.; Walton, R. A. *Multiple Bonds Between Metal Atoms*; Wiley-Interscience: New York, 1982.
(9) Herzog, S.; Kalies, W. *Z. Anorg. Allg. Chem.* **1967**, *351*, 237.
(10) Cotton, F. A.; Rice, C. E.; Rice, G. W. *J. Am. Chem. Soc.* **1977**, *99*, 4704.

Table I. FTIR Data for Trifluoroacetate Bridges and Donor Functional Groups (All Absorbances in cm^{-1})[a]

	ν_{CO_2}, asym			functional	functional group absorbance	
	η^1	η^2	ν_{CO_2}, sym	group	free	complexed
$Rh_2(tfa)_4(EtOH)_2$[b]		1664	1467			
$Mo_2(tfa)_4$[c]	1680	1592	1459			
$Cr_2(tfa)_4(Et_2O)_2(CH_2Cl_2)$		1680	1480	O—C—O	1115	1053
$Cr_2(tfa)_4(Et_2O)_2$ (mull)		1682	1484	O—C—O		1055
$Cr_2(tfa)_4(DMA)_2$	1717	1684	1476	C=O	1651	1606
$Cr_2(tfa)_4(Et_3PO_4)_2$		1682	1478	P—O—C	1034	1037
					979	984
$Cr_2(tfa)_4(DMCA)_2$		1681	1477	C=N	2217	2239
$Cr_2(tfa)_4(DMSO)_2$		1680	1478	S=O	1057	1012
		(1708)[d]				1022
$Cr_2(tfa)_4(Me_3PO)_2$		1681	1473	P=O	1179	1134
		(1712)[d]				
$Cr_2(tfa)_4(HMPA)_2$		1685	1473	P=O	980	992
$Cr_2(tfa)_4(DMTF)_2$		1679	1478	*e*	1538	1563
$Cr_2(tfa)_4(DMF)_2$		1680	1477	C=O	1676	1562
$Cr_2(tfa)_4[(MeO)_3P]_2$		1681	1477	*e*		
$Cr_2(tfa)_4(Me_4Urea)_2$		1685	1477	C=O	1640	1581

[a] DMA = dimethylacetamide, DMCA = *N,N*-dimethylcyanamide, DMTF = dimethylthioformamide, DMF = dimethylformamide, $(MeO)_3P$ = trimethyl phosphite, Me_4Urea = tetramethylurea. [b] Reference 9. [c] Reference 10. [d] Slow oxidation follows complexation as evidenced by shift in asymmetric stretch and color change from violet to green over a 24-h period. [e] Ligand vibrations shifted but specific shifts not assigned.

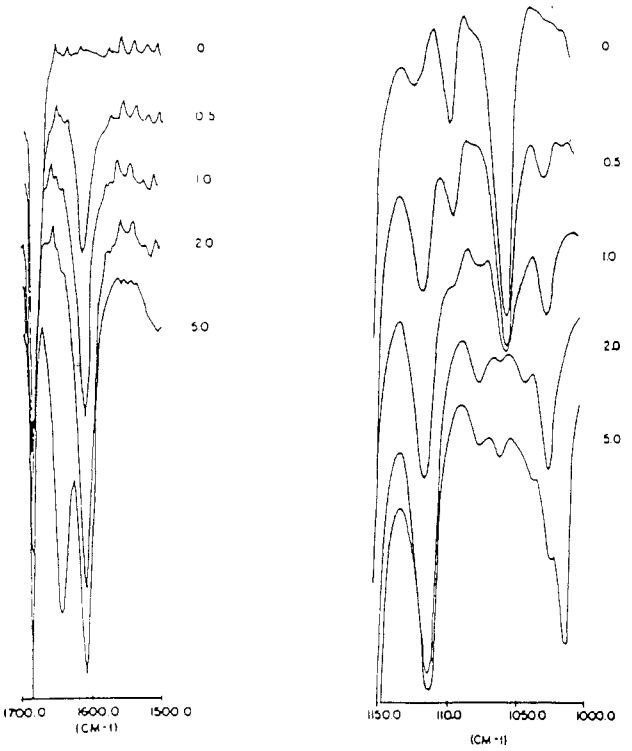

Figure 2. FTIR titration of I (8.9×10^{-3} M in CH_2Cl_2) with 0, 0.5, 1.0, 2.0 and 5.0 equiv of DMA: bound DMA, ν_{CO} = 1610 cm^{-1}; free DMA, ν_{CO} = 1639 cm^{-1}; bound Et_2O, ν_{COC} = 1053 cm^{-1}; free Et_2O, ν_{COC} = 1113 cm^{-1}.

These studies show that in solution two equilibria occur during the first isosbestic point:

$$Et_2OCr_2(O_2CCF_3)_4 + B \rightleftarrows 1{:}1$$

$$(Et_2O)_2Cr_2(O_2CCF_3)_4 + B \rightleftarrows 1{:}1 + Et_2O$$

As shown previously, these three species connected by equilibria can give a single isosbestic point.[11]

Over the concentration region corresponding to 2:1 adduct formation, the species $(Et_2O)Cr_2(O_2CCF_3)_4B$, $Cr_2(O_2CCF_3)_4B$, and $Cr_2(O_2CCF_3)_4B_2$ are all connected via equilibria.

The strong, sharp absorbances for the infrared asymmetric and symmetric carboxylate stretches of the trifluoroacetates can differentiate unidentate, ionic, bidentate, or bridging coordination.[12,13] The bridging carboxylate asymmetric and symmetric stretches of $Cr_2(tfa)_4(Et_2O)_2$ in methylene chloride occur at 1680 and 1480 cm^{-1}. A large excess (50 equiv) of DMA leads to a monodentate asymmetric carboxylate stretch at 1717 cm^{-1} assigned to an A_2B_3 species (eq 6) with equatorial coordination of DMA. Infrared results for methylene chloride solutions of $Cr_2(tfa)_4(Et_2O)_2$ (ca. 5×10^{-2} M) with 2 equiv of donor are given in Table I. With 2 equiv added, peak areas demonstrate 90% or greater complexation of DMA, Et_3PO_4, *N,N*-dimethylcyanamide (DMCA), dimethyl sulfoxide (DMSO), hexamethylphosphoramide (HMPA), and DMTF. A 1:1 equilibrium process ($AB + B \rightleftarrows AB_2$) with initial concentrations of 5×10^{-2} M going to ≥90% completion yields $K_2 \geq 1800$. Unfortunately, absorbance changes are too slight to allow satisfactory definition of K_1 by spectroscopy.[14]

Table II. Thermodynamic Data for the Exchange Reaction of $Cr_2(tfa)_4(Et_2O)_2$ with Donors

base	K_1[a]	K_2[a]	$-\Delta H_{1:1}$,[b] kcal mol^{-1}	$-\Delta H_{2:1}$,[b] kcal mol^{-1}
DMTF	1×10^5	500	1.89 (0.1)	1.80 (0.1)
DMCA	1×10^8	3×10^3	3.75 (0.1)	2.66 (0.2)
DMF	1×10^8	1×10^4	4.52 (0.3)	3.01 (0.5)
$(MeO)_3P$	1×10^8	2×10^3	0.79 (0.1)	0.73 (0.1)
$(EtO)_3PO$	1×10^{10}	1×10^6	4.37 (0.2)	3.05 (0.3)
DMA	1×10^9	1×10^5	5.26 (0.2)	3.59 (0.4)
DMSO	1×10^9	6×10^4	5.58 (0.3)	3.95 (0.5)
Me_3PO[c]	1×10^7	2×10^4	5.95 (0.3)	6.55 (0.4)
HMPA	1×10^{11}	6×10^6	5.97 (0.2)	5.48 (0.4)

[a] The equilibrium constants are those values that minimize the standard deviations of $\Delta H_{1:1}$ and $\Delta H_{2:1}$, solved from the calorimetric data. [b] Values in parentheses are conditional standard deviations. [c] Data are not reliable due to complicating side reactions.

B. Calorimetry. Table II contains the results of the calorimetric titrations. The enthalpies of the second exchange, $\Delta H_{2:1}$, are consistently lower than those for the first, $\Delta H_{1:1}$, in all cases except that for Me_3PO. The change in solution color to green and continued heat evolution when Me_3PO is added above a 2:1 molar ratio indicates oxidation of the chromium, probably via oxygen atom transfer from the phosphine oxide.

Thermodynamic studies conducted in methylene chloride solvent, S, need to be corrected for solvation effects.[15] The individual

(11) Mayer, R. G.; Drago, R. S. *Inorg. Chem.* **1976**, *15*, 2010.

(12) Garner, C. D.; Hughes, B. *Adv. Inorg. Chem. Radiochem.* **1975**, *17*, 1.
(13) Girolami, G. S.; Mainz, V. V.; Andersen, R. A. *Inorg. Chem.* **1980**, *19*, 805.
(14) Guidry, R. M.; Drago, R. S. *J. Am. Chem. Soc.* **1973**, *95*, 6645.

Table III. Experimental and Calculated Solvation-Corrected Enthalpies

base (E, C)	$-\Delta H_{1:1}^{cor}$,[a] kcal mol^{-1}	$-\Delta H_{1:1}^{calcd}$,[a] kcal mol^{-1}	$\Delta H_{2:1}^{cor}$,[c] kcal mol^{-1}	$\Delta H_{2:1}^{calcd}$,[d] kcal mol^{-1}
Et_2O (1.08, 3.08)	0	0	0	0
DMCA (1.06, 1.74)	5.5 (0.1)	5.4	4.4 (0.2)	4.2
DMF (1.24, 2.47)	6.5 (0.3)	6.7	5.0 (0.5)	5.3
DMA (1.32, 2.48)	7.4 (0.2)	7.3	5.8 (0.4)	5.8
DMSO (1.36, 2.78)	7.8 (0.3)	7.5	6.2 (0.5)	6.0
$(CH_3O)_3P$ (0.73, 6.47)	1.8 (0.1)	1.8	1.7 (0.1)	1.7
$(EtO)_3PO$ (1.20, 1.84)	6.4 (0.2)	6.5	5.0 (0.3)	5.1
HMPA (1.52, 3.80)	8.4	8.5	7.9 (0.4)	6.8

[a] Solvation corrected for the hydrogen bonding of the base to CH_2Cl_2 by using the newly[16d] refined $E' = 1.71$ and $C' = -0.04$ parameters. Quantity in parentheses is the conditional standard deviation for the measured uncorrected heats. [b] Calculated from (1) by using the E_B and C_B values from ref 16d. E_A, C_A, and W were determined from a fit of the $\Delta H_{1:1}$ values in Table I. Values of 7.79, −0.23, and 2.4 are respectively obtained for E_A, C_A, and W. The heat calculated by using only E_A and C_A is that for "$(Et_2O)Cr_2(tfa)_4$" picking up a base. The tabulated enthalpies were calculated by substituting the W, E_A, and C_A values for $Et_2OCr_2(tfa)_4$ into (1) along with the E_B and C_B values for the base given in column 1 in parentheses. This produces the solvent-corrected ether displacement enthalpy with a small contribution from $Et_2OCr_2(tfa)_4$ being balanced by some ether displacement from $BCr_2(tfa)_4Et_2O$. The E and C parameters of $(EtO)_3PO$ are poorly defined, so modified E values were calculated to fit the 1:1 enthalpies. Consequently this system does not constitute a check on the 1:1 enthalpies but provides us another system for analysis of the 2:1 data. Since the C/E ratios for the 1:1 and 2:1 adducts are similar, these E_B and C_B values should have predictive ability for the 2:1 reaction. [c] The experimental enthalpies for the 2:1 adduct formation ether displacement reaction corrected for desolvation of the base by CH_2Cl_2. [d] Calculated from (14) by using $k = 0.998$, $k' = -0.039$, and $w = 3.58$. The data for HMPA was inconsistent with the other data used in the determination of k and k'. Apparently, an excess of the stronger HMPA donor leads to some of the reactivity problems found with pyridine.

enthalpy components to the measured 1:1 and 2:1 enthalpies are specified in (7) and (8). Here ΔH_1 and ΔH_5 represent the

$$(Et_2O)Cr_2\overset{\Delta H_1}{\text{—}}(Et_2O) + B\overset{\Delta H_2}{\text{—}}S \rightleftharpoons (Et_2O)Cr_2\overset{\Delta H_3}{\text{—}}B + Et_2O\overset{\Delta H_4}{\text{—}}S \quad (7)$$

$$(Et_2O)\overset{\Delta H_5}{\text{—}}Cr_2B + B\overset{\Delta H_2}{\text{—}}S \rightleftharpoons B\overset{\Delta H_6}{\text{—}}Cr_2B + Et_2O\overset{\Delta H_4}{\text{—}}S \quad (8)$$

enthalpy of dissociation of ether and ΔH_3 and ΔH_6 the enthalpy of binding the base.

The solvation contributions, ΔH_2 and ΔH_4, could be calculated from the E_B and C_B values for the various donors and the E'_A, C'_A, and W values for methylene chloride of 1.71, −0.04, and 0, by using (1). However, an unknown amount of Et_2O is dissociated when $Cr_2(tfa)_4(Et_2O)_2$ is dissolved in CH_2Cl_2. Since the displacement of ether and solvation of the displaced ether is a constant whose value is unknown, we will not correct the enthalpies for ether solvation but will include it in our constant W term. The displacement enthalpies corrected for ΔH_2, desolvation of the base from CH_2Cl_2, are listed in Table III as ΔH^{cor} and defined in (9) and (10), where n and n' represent the fraction of the total dimer

$$\Delta H_{1:1}^{cor} = \Delta H_{1:1} + \Delta H_2 = \Delta H_3 + n\Delta H_4 - n\Delta H_1 \quad (9)$$

$$\Delta H_{2:1}^{cor} = \Delta H_{2:1} + \Delta H_2 = \Delta H_6 + n'\Delta H_4 - n'\Delta H_5 \quad (10)$$

present as the dietherate and $BCr_2(tfa)_4Et_2O$, respectively. The donor E_B and C_B values for DMTF and Me_3PO were determined from a limited data set and were not well-defined enough to confidently predict enthalpies. To alleviate propagation of their uncertainties, these heats are not used in the following analysis.

C. Quantitative Analysis. The E and C parameters for an acid (or base) can be solved[16] from the enthalpies of adduct formation with a series of bases (or acids) by using the E, C, and W equation (eq 1). Substituting the solvent-corrected experimental heats (eq 9; Table III) into (1) gives simultaneous equations of the form shown in (11), where the R_2O notation indicates acid parameters

$$-\Delta H_{1:1}^{cor} = -\Delta H_3 + n\Delta H_1 - n\Delta H_4 = E_A^{R_2O}E_B + C_A^{R_2O}C_B \quad (11)$$

for the mono(ether) adduct, $(Et_2O)Cr_2(O_2CCF_3)_4$, binding to bases ($-\Delta H_3$) and W is $n\Delta H_1 - n\Delta H_4$, the constant enthalpy for displacing the unknown amount of ether and solvating it with CH_2Cl_2:

$$Et_2O(Cr_2)Et_2O \overset{CH_2Cl_2}{\rightleftharpoons} Et_2O(Cr_2) + Et_2O(CH_2Cl_2)$$

Solving six equations for the six donors whose E_B and C_B are well-defined[16] allows calculation of the constant contribution, $W = n\Delta H_1 - n\Delta H_4$, and the $E_A^{1:1}$ and $C_A^{1:1}$ associated with the mono(ether) adduct. The best-fit parameters are $E_A^{1:1} = 7.79$, $C_A^{1:1} = -0.23$, and $W = 2.4$ kcal mol^{-1}. These E_A and C_A parameters are slightly (~10%) larger than those for $Cr_2(O_2CCF_3)_4 \cdot Et_2O$ because of the slight dissociation of ether from the dietherate in CH_2Cl_2 solution. This effect is compensated by the slight dissociation of Et_2O from $BCr_2(tfa)_4Et_2O$. The parameters do permit the calculation of the experimental enthalpies for the displacement reaction that occurs when the dietherate is dissolved in CH_2Cl_2. The experimental enthalpies and those calculated from (11) are given in Table III. This approach has enabled us to calculate ideal solvation-minimized data for the displacement reaction from nonideal conditions.

In order to compare the chromium dimer to other metal carboxylates, we need to have E and C values for $Cr_2(O_2CCF_3)_4$ and not those reported above for "$(Et_2O)Cr_2(O_2CCF_3)_4$". We can obtain this information from eq 2 and 3 if we can obtain k and k', for then only E_A and C_A will remain as unknowns. In previous work where the free acid is studied, E_A, C_A, k, and k' are known and $E_A^{1:1}$ and $C_A^{1:1}$ are calculated for various base adducts. This comparison as well as our desire to compare the inductive transfer parameters, k and k', for the chromium–chromium bond, led us to the evolution of a procedure to determine these constants on this system. The $\Delta H_{2:1}$ displacement enthalpies (Table II) are corrected for base solvation by using E' and C' for CH_2Cl_2 leading to $\Delta H_{2:1}^{cor}$ (Table III). In terms of the ether displacement reaction we write

$$-\Delta H_{2:1}^{cor} + W = E_A^{1:1}E_B + C_A^{1:1}C_B \quad (12)$$

Here, $E_A^{1:1}$ and $C_A^{1:1}$ are parameters for $BCr_2(tfa)_4$, and W is the enthalpy for displacing ether from $BCr_2(tfa)_4Et_2O$ and solvating it by CH_2Cl_2. The term $E_A - kE_B$ provides the $E_A^{1:1}$ value for $BCr_2(tfa)_4$ according to (2), and in a similar fashion, (3) describes $C_A^{1:1}$ leading to

$$-\Delta H_{2:1}^{cor} + W = (E_A - kE_B)E_B + (C_A - k'C_B)C_B \quad (13)$$

where E_A and C_A refer to parameters of the naked dimer ($Cr_2(tfa)_4$). From our study of the 1:1 adducts we know that

$$E_A^{R_2O} = 7.79 = E_A - kE_{Et_2O} \quad \text{or} \quad E_A = 7.79 + k(1.08) \quad (14a)$$

$$C_A^{R_2O} = -0.23 = C_A - k'C_{Et_2O} \quad \text{or} \quad C_A = -0.23 + k'(3.08) \quad (14b)$$

Table IV. Acid Parameters for Dinuclear Metal Carboxylates[a]

	E_A	C_A	k	k'
$Mo_2(pfb)_4$	6.29	0.19	1.56	0.0084
$Rh_2(but)_4$	3.55	1.20	1.12	0.0269
$Cr_2(tfa)_4$	7.79	−0.23	0.998	−0.039

[a] These parameters are consistent with the newly refined set reported in ref 16d.

(15) Drago, R. S.; Nusz, J. A.; Courtright, R. C. *J. Am. Chem. Soc.* **1974**, *96*, 2082.

(16) (a) Drago, R. S. *Struct. Bonding (Berlin)* **1973**, *15*, 73. (b) Drago, R. S. *Pure Appl. Chem.* **1980**, *52*, 2261. (c) Drago, R. S. *Coord. Chem. Rev.* **1980**, *33*, 251. (d) Drago, R. S.; Wong, N.; Bilgrien, C.; Vogel, G. C. *Inorg. Chem.* **1987**, *26*, 9.

Making those substitutions into (13) and rearranging lead to

$$-\Delta H_{2:1}^{cor} + W - 7.79E_B + 0.23C_B = kE_B(1.08 - E_B) + k'C_B(3.08 - C_B) \quad (15)$$

Substituting the enthalpies, and the corresponding C_B and E_B for different bases into (15) produces simultaneous equations that can be solved for W, k, and k'. The data and the best-fit parameters are given in Table III. The best-fit values are $k = 0.998$, $k' = -0.039$, and $W = 3.58$. These parameters demonstrate the ability of the metal–metal bond to transmit electrostatic (k) and covalent (k') effects in $Cr_2(tfa)_4$. Equations 2 and 3 may now be solved for E_A and C_a since all other quantities are known to produce values for the naked chromium dimer, $Cr_2(tfa)_4$. The derived E_A and C_A values along with those previously determined for the molybdenum and rhodium dimers are given in Table IV.

The large E_A and very small (negative[17]) C_A values for the chromium dimer demonstrate relatively strong Lewis acidity and a tendency to interact with Lewis bases in primarily an ionic fashion. The low C would be consistent with a higher energy LUMO for chromium that mixes less effectively with the donor orbital (poorer energy match). The large E corresponds to the partial metal positive charge being concentrated on a smaller chromium center compared to molybdenum and rhodium. The low k' value, which corresponds to transmission of the base covalent parameters, indicates that even though base binding weakens the metal–metal bond it does not serve to polarize the bonding density in the chromium–chromium bond toward the other center, consistent with poor orbital overlap between the two metal centers. The value of k, which corresponds to transmission of the coordinated base electrostatic parameter, is the smallest of the three acids. Electrostatic interaction of the base dipole on one side with the second metal center and with the second base dipole should vary as $1/r^2$. Of the three systems studied, the chromium dimer exhibits the longest metal–metal bond (2.54 Å for[7] $Cr_2(tfa)_4(Et_2O)_2$, 2.39 Å for[18] $Rh_2Ac_4(H_2O)_2$, and 2.09 Å for[18] $Mo_2(tfa)_4$) and should, as found, exhibit the smallest base electrostatic transfer to the second site.

D. Magnetic Susceptibility. 1. Solution Studies. Theoretical investigations on dichromium tetraformate at the SCF level have predicted both the quadrupole bond, $\sigma^2\pi^4\delta^2$, and no bond, $\sigma^2\delta^2\delta^{*2}\sigma^{*2}$, configurations, neither of which corresponds to a realistic description.[19] Incorporation of correlation effects[20] gives importance to the $\sigma^2\pi^4\delta^2$ term and a ground-state bond order close to 1.5. Dichromium tetraacetate is diamagnetic,[21] and Zerner has proposed two antiferromagnetically coupled chromium centers with no net covalency between the chromium atoms as the dominant description; however, unrealistically long Cr–Cr distances are predicted.[22] At shorter, (1.8–2.5 Å) experimental bond lengths, d-orbital overlap is expected, and Zerner suggests that some degree of covalency accompanies the antiferromagnetic description.

The trifluoroacetate-bridged dimer studied here may represent just such a borderline example with a chromium–chromium separation of 2.54 Å. An early magnetic study[9] reported magnetic moments of $\mu_{eff} = 0.74\ \mu_B$ for "$Cr(F_3CCOO)_2$" and 0.85 μ_B for "$Cr(F_3CCOO)_2$·ether".

The room-temperature magnetic susceptibilities of various adducts of the form $Cr_2(tfa)_4L_2$ were investigated by using the solution Evans method,[23] by generating the complexes in situ. The molar magnetic susceptibilities and moments calculated from the observed frequency shifts are reported in Table V. A trend toward larger susceptibilities with increasing donor strength provides the first conclusive evidence for genuine paramagnetism in a series of chromium carboxylates since this consistency would not be observed with random trace contamination by Cr(III) impurities.[8]

Table V. Magnetic Susceptibilities and Moments for $Cr_2(tfa)_4B_2$ Species, at 20 °C (Evans Method)

	concn, mM	$\Delta\nu$, Hz	$10^4\chi_M$[a]	μ_{eff},[b] μ_B
$Rh_2(tfa)_4(THF)_2$	26.2	0	0	0
$Cr_2(tfa)_4(Et_2O)_2$	28.4	3.54	6.66	0.89
$Cr_2(tfa)_4[(MeO)_3P]_2$	46.9	6.77	6.91	0.91
c	50.4	7.32	6.95	0.91
$Cr_2(tfa)_4(Et_3PO_4)_2$[d]	61.3	13.24	10.94	1.15
$Cr_2(tfa)_4(DMTF)_2$[d]	62.1	13.98	12.40	1.22
$Cr_2(tfa)_4(Me_4Urea)_2$	51.1	15.38	14.53	1.32
$Cr_2(tfa)_4(DMF)_2$[d]	21.3	17.64	18.18	1.48
$Cr_2(tfa)_4(DMSO)_2$[d]	62.2	24.66	20.73	1.58
$Cr_2(tfa)_4(DMA)_2$[d]	62.1	24.84	20.80	1.58
$Cr_2(tfa)_4(DMCA)_2$	27.2	20.50	36.90	2.11
c	88.3	62.20	34.52	2.04
$Cr_2(tfa)_4(HMPA)_2$	17.7	17.64	47.01	2.38
$Cr_2(tfa)_4(Me_3PO)_2$	20.9	33.20	77.86	3.06

[a] Per dimer, ±1 × 10^{-4}. [b] Per Cr(II) atom, ±0.35 μ_B. [c] Multiple determinations. [d] Determination in CD_2Cl_2.

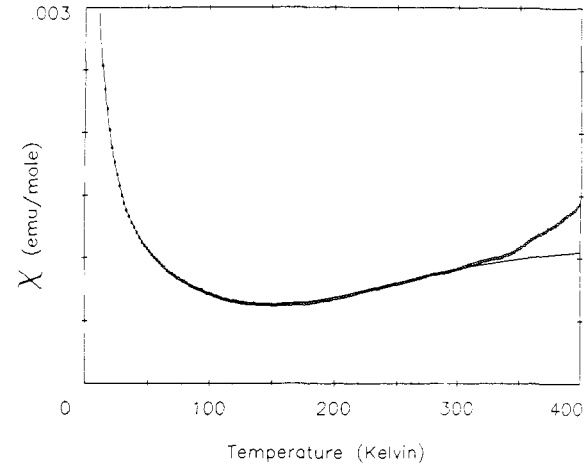

Figure 3. Experimental and calculated χ vs T plot for $Cr_2(O_2CCF_3)_4(hmpa)_2$. $g = 2.05$, $E = 611$ cm^{-1}, TIP = 0.000 30, % imp = 1.3, and $\Theta = -4.8$.

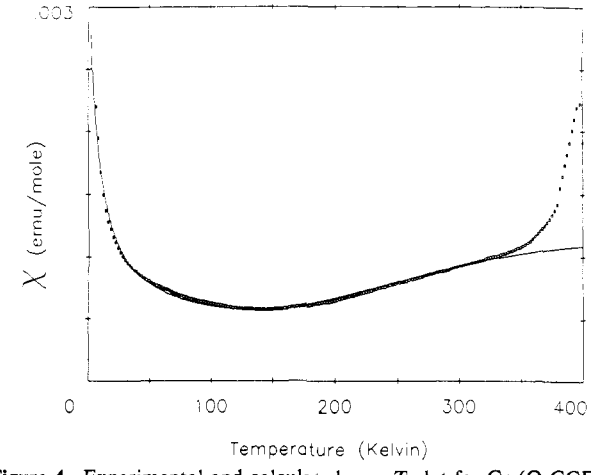

Figure 4. Experimental and calculated χ vs T plot for $Cr_2(O_2CCF_3)_4(Et_2O)_2$. $g = 2.06$, $E = 622$ cm^{-1}, TIP = 0.000 38, % imp = 0.8, and $\Theta = -8.10$.

(17) The negative C_A value does not imply that the dimer interacts covalently in an antibonding sense but simply that this is the best-fit parameter to a data set in which implicit assumptions have been made in defining the magnitudes of the original parameters. For all intensive purposes, the C_A value merely suggests little covalent interaction between $Cr_2(tfa)_4$ and donors.

(18) Cotton, F. A.; Norman, J. G., Jr. *J. Coord. Chem.* **1971**, *1*, 161.
(19) Mitschler, A.; Rees, B.; Wiest, R.; Benard, M. *J. Am. Chem. Soc.* **1982**, *104*, 7501.
(20) Atha, P. M.; Hillier, I. H.; Guest, M. F. *Mol. Phys.* **1982**, *46*, 437.
(21) Figgis, B. N.; Martin, R. L. *J. Chem. Soc.* **1956**, 3837.
(22) deMello, P. C.; Edwards, W. D.; Zerner, M. C. *Int. J. Quantum Chem.* **1983**, *23*, 425.
(23) Evans, D. F. *J. Chem. Soc.* **1959**, 2003.

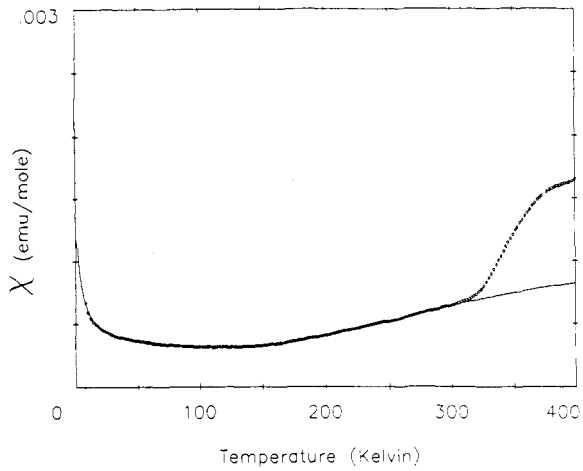

Figure 5. Experimental and calculated χ vs T plot for $Cr_2(O_2CCF_3)_4(Et_3PO_4)_2$. $g = 2.05$, $E = 688$ cm^{-1}, TIP = 0.000 28, % imp = 0.1, and $\Theta = -2.7$.

The measured susceptibilities roughly parallel the experimental enthalpies except for the DMCA adduct, which displays a larger moment than expected.

2. Solid-State Magnetic Studies. The magnetic data corrected for diamagnetism with Pascal's constants are tabulated in the supplementary material and are illustrated in Figures 3–5 as plots of susceptibility versus temperature. Each of the three complexes exhibits similar magnetic behavior.

The features of the magnetic susceptibility curves can be divided into three temperature regions. At the lower temperatures ($T < 150$ K) a small amount of residual paramagnetism becomes the dominant magnetic contribution as the temperature is lowered to the experimental limit. The intermediate-temperature region ($150 \text{ K} < T < 310$ K) exhibits a gradual rise in the magnetic susceptibility as the temperature is *increased*. Upon further heating of the sample, the high-temperature region ($T > 310$ K) is characterized by a more rapid increase in the magnetic susceptibility of the chromium(II) dimers.

The theoretical analysis of the magnetic susceptibility of the chromium binuclear complexes must first account for the presence of the paramagnetic impurities. The low-temperature paramagnetic component of the magnetic susceptibility data is consistent with a monomeric chromium(II) impurity with spin $S = 2$. The magnetic contribution of the monomer impurity may be readily predicted by using the Curie–Weiss law. A spin $S = 2$ system might be expected to exhibit a crystal field splitting of the multiplet, and this would give rise to a nonnegligible value for the Weiss constant. The theoretical magnetic susceptibility data calculated for the binuclear chromium(II) ions were corrected for the presence of the monomeric impurity by using (16), where

$$\chi = (1 - P)\chi_B + 2P\chi_{cw} \qquad (16)$$

χ is the calculated total susceptibility, χ_B is the binuclear susceptibility, χ_{cw} is the Curie–Weiss magnetic susceptibility expected for the impurity ($\chi_{cw} = 2Ng^2\mu_B^2/k(T - \Theta)$) and P is the fraction of monomeric impurity.

At the highest temperature ($T > 310$ K), an anomalous and rather abrupt increase in the magnetic susceptibility of the samples occurs. This behavior is the result of the thermal decomposition of the samples above room temperature. Each of the samples shows an appreciable weight loss following the 6–400 K magnetic measurement, and a visual inspection of the samples confirmed their decomposition during the high-temperature heating cycle. The sample decomposition most likely follows the loss of the loosely coordinated axial ligand; however, no further analysis of the decomposition products was attempted. Our theoretical analysis of the magnetic data was limited to temperatures below the onset of decomposition.

The temperature region from about 150 K to the onset of decomposition contains the magnetic data of most interest to our analysis. The increase in the magnetic susceptibility exhibited by these complexes as the temperature increases toward room temperature can be interpreted in terms of the metal–metal bonding between the two chromium(II) ions.

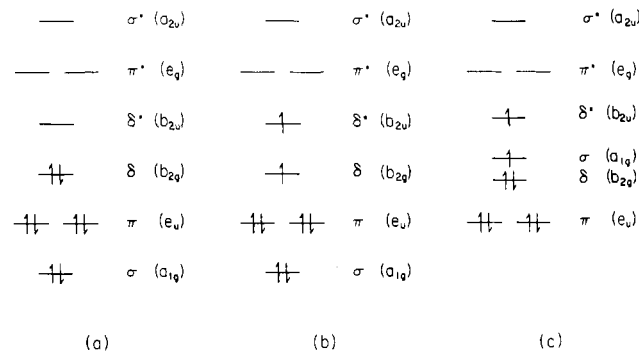

Figure 6. Molecular orbital energy orderings from d-orbital combinations in chromium(II) dimers: (a) diamagnetic strong metal–metal bond; (b) paramagnetic weak δ bond; (c) paramagnetic weak metal–metal σ bond.

Table VI. Parameters Obtained for the Best Fit of (16) and (17) to the Magnetic Susceptibility Data for the Chromium Dimers[a]

complex	g	E, cm^{-1}	TIP, emu/mol	P	Θ, K	T_d, K
$Cr_2(tfa)_4(Et_3PO_4)_2$	2.08	689	0.000 27	0.002	−4.4	320
$Cr_2(tfa)_4(Et_2O)_2$	2.08	626	0.000 39	0.007	−7.5	340
$Cr_2(tfa)_4(hmpa)_2$	2.05	615	0.000 31	0.013	−4.8	340

[a] E is the energy of the $^3A_{2u}$ excited state, TIP is the underlying temperature-independent paramagnetism due to each chromium(II) ion, P is the fraction of monomeric (Curie Law) impurity, Θ is the Weiss constant of the impurity, and T_d is the onset of decomposition of the samples. All parameters (except T_d) were allowed to vary.

Figure 6 contains molecular orbital energy level diagrams for the metal–metal bonding with eight electrons (four from each chromium(II) ion) assigned to these orbitals. The entire binuclear complex has D_{4h} symmetry with a ground-state energy level (Figure 6a) of $^1A_{1g}$ symmetry and a ($a_{1g}^2e_u^4b_{2g}^2$) molecular orbital configuration corresponding to a metal–metal bond of order 4 (one σ bond, two π bonds, and one δ bond) and a diamagnetic complex. When base is coordinated to an axial position (including aggregation that exists in the solid), the metal–metal bond weakens. Paramagnetism can arise by thermal population of the excited state with a ($a_{1g}^2e_u^4b_{2g}^1b_{1u}^1$) molecular orbital electron configuration (Figure 6b) and $^3A_{2u}$ symmetry. This state will have a formal triple bond (one σ bond, two π bonds, half of a δ bond, and half of a δ^* antibond) and will have a triplet spin multiplicity. Alternatively, base coordination could weaken the σ-metal–metal overlap by utilizing the d_{z^2} orbital to bond the base, breaking the metal–metal σ bond and leading to the $^3A_{2u}$ configuration described in Figure 6c or one of higher multiplicity. The actual system may correspond to populations of Figure 6a–c.

Our theoretical analysis of the magnetic data includes only the $^1A_{1g}$ ground state and the lowest excited $^3A_{2u}$ state. Other excited electron configurations were not required to obtain a theoretical fit to the experimental data. The electrons of the $^3A_{2u}$ excited state may be assigned a triplet basis set of wave functions ($\psi_{^3A_{2u}} = <1, <0, <-1$). The application of the Van Vleck equation (eq 12) to this basis set will generate a closed-form solution that allows the calculation of the magnetic susceptibility for this system.

$$\chi_B = \frac{Ng^2\mu_B^2}{kT}\,\frac{2e^{-E/kT}}{1 + 3e^{-E/kT}} + \text{TIP} \qquad (17)$$

In (17), E represents the energy that separates the $^3A_{2u}$ energy level from the $^1A_{1g}$ ground state ($-2J$), TIP is the underlying temperature-independent paramagnetism of the chromium(II) ions, and the other parameters have their usual meaning.

The magnetic data of the complexes were fitted over temperatures up to the onset of thermal decomposition by using five variables for the magnetic analysis: the g value, the triplet energy (E), the temperature-independent paramagnetism (TIP), the

fraction of monomeric impurity (P), and the Weiss parameter for the monomer (Θ). The curves drawn through the data points in Figures 3–5 are the best fits of the magnetic data to (16) and (17) using the parameters listed in Table VI. The magnetic data were also fit with only four parameters by constraining the g value to 2.0. The fits were of similar quality, but in each case the triplet energy was 10 cm^{-1} less.

The only other first-row transition-metal carboxylate dimer whose susceptibility is reported as a function of base coordination is copper(II).[24] The long Cu–Cu distance (2.6–2.9 Å), magnetic behavior, and odd electron population of the $d_{x^2-y^2}$ orbitals suggest a superexchange pathway through the carboxylate bridge. The value of $-2J$ is sensitive to axial ligation, generally increasing as the terminal ligands become stronger electron-pair donors.[25] At a given temperature, larger values of $-2J$ would give smaller experimental moments.

The thermal population of low-lying antibonding orbitals is observed[26] in β-Mo_2Cl_4(dmpe) (dmpe = 1,2-bis(dimethylphosphino)ethane), which has a 40° twist angle, but is not observed in the eclipsed "rotamer" $Mo_2Cl_4(PMe_3)_4$. Values of $-2J$ = 400–500 cm^{-1} are reported for the former and are an order of magnitude greater for the latter. A series of dimolybdenum(III) molecules with RS groups has also been reported[27] to have magnetic properties consistent with the thermal population of a $\delta\delta^*$ orbital to give a triplet state.

The chromium dimers exhibit some degree of orbital overlap, suggested to be incomplete in the $Cr_2(tfa)_4(Et_2O)_2$ adduct. The data in Table V suggest a direct exchange mechanism. In the Cu(II) systems in which the superexchange pathway predominates, better donors give smaller magnetic moments. The reverse is true for the chromium series studied here. Donor lone pairs interact primarily with the chromium dimer σ^* orbitals. Stronger donors would serve to destabilize the Cr–Cr σ, δ, and σ^* orbitals while stabilizing the Cr–Cr δ^* orbitals. The resulting partial population of δ^* is consistent with the observed trend for larger moments with better donors. Additionally, the calculated single–triplet splittings (611–688 cm^{-1}) lie above the range found for the copper carboxylates[25] (217–555 cm^{-1}), indicating a more efficient exchange mechanism in the chromium carboxylates.

Experimental Section

All syntheses, manipulations, and data collection were conducted under inert atmosphere by using standard Schlenk techniques or a Vacuum Atmospheres glovebox.

Solution Spectral Studies. FTIR spectra were recorded on a Nicolet 5DX-B spectrometer. FT NMR spectra were collected on a JEOL XL-100 instrument. For magnetic susceptibility determinations, solutions were prepared by addition of 2.2–3 equiv of the donor of interest to (1–5) $\times 10^{-2}$ M solutions of $Cr_2(tfa)_4(Et_2O)_2$. A coaxial tube arrangement was used, which contained a solvent system of 2% v/v C_6H_6 and 2% v/v TMS in C_6D_6 in both the outer 5-mm tube and the inner 1-mm capillary. The inner capillary also contained the paramagnetic species at a concentration of ca. 5×10^{-2} M.

For our calculations we used a form of the molar susceptibility equation given by Brault and Rougee,[28] modified to include the density correction term[29]

$$\chi_M = \frac{3 \times 10^3(\Delta\nu)}{2\pi\nu C} + \chi_0 M - \chi_D + \frac{10^3\chi_0(d_0 - d_s)}{C} \qquad (18)$$

where χ_M is the molar magnetic susceptibility, $\Delta\nu$ is the experimental frequency shift separation in hertz, ν is the spectrometer frequency (99.55 MHz), C is the molar concentration of the paramagnetic substance, χ_0 is the mass susceptibility of the solvent, M is the molecular weight of the paramagnetic complex, χ_0 is the diamagnetic suscepbility of the complex, and d_0 (d_s) is the density of the solvent (solution). The magnetic moment is expressed in Bohr magnetons. χ_M is a molar quantity, calculated per mole of dimer, while μ_{eff} is determined per mole of metal atom and must be determined from $^1/_2\chi_M$.

The diamagnetic complex $Rh_2(tfa)_4(THF)_2$ gave no shift or asymmetry in the TMS or C_6H_6 peaks. The sum of the diamagnetic term and density correction then is -5.63×10^{-4} (obtained by setting both χ_M and $\Delta\nu$ equal to zero). The calcuated diamagnetic term is -3.0×10^{-4} (from Pascal's constant,[30] where each Rh(II) is given a value of -20×10^{-6} mL mol^{-1}), and the difference approximates the density correction. An upper error limit on the shift determination is about 0.3 Hz, which corresponds to a 0.43×10^{-4} contribution to the diamagnetic/density term. Substitution of the value for the combined complex diamagnetism plus density correction into the modified Evans equation gives

$$\chi_M = \frac{3 \times 10^3(\Delta\nu)}{2\pi\nu C} + \chi_0 M + 5.63 \times 10^{-4} \qquad (19)$$

At the concentrations used, complex precipitation warranted shift determination in CD_2Cl_2 in several instances. Equation 16 was used to calculate the molar magnetic susceptibilities from both the C_6D_6 and CD_2Cl_2 solution data. The attendant error is estimated to be about 1×10^{-4}. Use of the "spin-out" formula for the molar susceptibility allows determination of the effective magnetic moment.

Adiabatic Calorimetry. It is best to determine the equilibrium constants that apportion the experimental heats and the molar enthalpies from separate experiments, since the four parameters K_1, K_2, $\Delta H_{1:1}$, and $\Delta H_{2:1}$ obtained calorimetrically are frequently highly correlated. However, enthalpies for two successive equilibria can be determined from exclusively calorimetric data provided that $K_1 \gg K_2$. From the calorimetric data, the best K_1, K_2 pair that minimized the enthalpy deviation from the experimental values was used to define $\Delta H_{1:1}$ and $\Delta H_{2:1}$.

Solid-State Magnetic Susceptibility. For solid-state magnetic measurements, polycrystalline samples weighing approximately 100 mg were placed in an airtight delrin sample container and then transferred to the susceptometer. Magnetic measurements were recorded by using the SHE VTS-50 superconducting SQUID susceptometer. Data were recorded over the 6–400 K temperature region at a measuring field of 5.0 kG. Measurement and calibration techniques are described elsewhere.[31]

Elemental analyses were performed by Galbraith Laboratories, Knoxville, TN. All bases and solvents were distilled from appropriate desiccant and either vacuum transferred or treated to three cycles of freeze–pump–thaw to remove oxygen.

Syntheses. Dichromium(II) Tetrakis(trifluoroacetate)–Bis(diethyl ether) (I). Chromous trifluoroacetate was prepared by a modified literature procedure.[32] Under dinitrogen, 5.5 g (9.9 mmol) of potassium chromous carbonate[33] and 8.0 mL (100 mmol) of trifluoroacetic acid were refluxed in 80 mL of diethyl ether for 6 h.

The Schlenk flask was plunged briefly into a dry ice bath, the purple ether layer decanted from the frozen blue aqueous layer, and the ether removed by vacuum. Extraction with benzene followed by two recrystallization from benzene and vacuum drying (30 min, 25 °C) produced purple blocks of $Cr_2(tfa)_4(Et_2O)_2$. Prolonged evacuation (>6 h) was found to strip off coordinated ether. Final yields were typically about 20%. Attempts to purify by sublimation decomposed the complex. Repeated elemental analyses typically showed loss of 5–10% coordinated diethyl ether. Anal. Calcd for $C_{16}H_{20}Cr_2F_{12}O_{10}$: C, 27.29; H, 2.85; Cr, 14.77. Found: C, 25.91; H, 2.82; Cr, 15.01.

Dichromium(II) Tetrakis(trifluoroacetate)–Bis(triethyl phosphate). A 490-mg (0.70-mmol) sample of I was dissovled in 20 mL of benzene, and 0.35 mL (2.1 mmol) of triethyl phosphate was added to give a deep blue solution. Volume was reduced to 5 mL, and the solution was cooled to 5 °C for 24 h to produce a mass of dark blue cubic crystals. Solid was collected, washed with cyclohexane, and vacuum-dried (25 °C) 30 min. Anal. Calcd for $C_{20}H_{20}Cr_2F_{12}O_{16}P_2$: C, 26.10; H, 3.29; F, 24.77. Found: C, 26.11; H, 3.40; F, 24.44.

Dichromium(II) Tetrakis(trifluoroacetate)–Bis(hexamethylphosphoramide). A 525-mg (0.74-mmol) sample of I was dissolved in 20 mL of benzene, and 0.30 mL (1.7 mmol) of hexamethylphosphoramide was added to give a deep blue solution. The solution was cooled to 5 °C and bright blue cubic crystals began to form after 15 min. After 24 h, the crystals were filtered and dried under a stream of dinitrogen. Anal. Calcd for $C_{20}H_{36}Cr_2F_{12}N_6O_{10}P_2$: C, 26.27; H, 3.97; F, 24.93; N, 9.19.

(24) Melnik, M. *Coord. Chem. Rev.* **1982**, *42*, 259.
(25) Jotham, R. W.; Kettle, S. F. A.; Marks, J. A. *J. Chem. Soc., Dalton Trans.* **1972**, 428.
(26) Cotton, F. A.; Diebold, M. P.; O'Connor, C. J.; Powell, G. L. *J. Am. Chem. Soc.* **1985**, *107*, 7438.
(27) Hopkins, M. D.; Zietlow, T. C.; Miskowski, W. M.; Gray, H. B. *J. Am. Chem. Soc.* **1985**, *107*, 510.
(28) Brault, D.; Rougee, M. *Biochemistry* **1974**, *13*, 4598.
(29) Desmond, M. J. Ph.D. Thesis, University of Illinois, 1980.
(30) Figgis, B. N.; Lewis, J. In *Modern Coordination Chemistry*; Lewis, J., Wilkins, R. G., Eds.; Interscience: New York, 1960.
(31) O'Connor, C. J. *Prog. Inorg. Chem.* **1982**, *29*, 203.
(32) Garner, C. D.; Hillier, I. H.; MacDowell, A. A.; Walton, I. B.; Guest, M. F. *J. Chem. Soc., Faraday Trans. 1* **1979**, 485.
(33) Ouahes, R.; Amiel, J.; Suquet, H. *Rev. Chim. Miner.* **1970**, *7*, 789.

Found: C, 26.34; H, 3.99; F, 24.38; N, 9.21.

Acknowledgment. We acknowledge support of this research by the National Science Foundation through Grant No. 86 18766.

Registry No. I, 15684-01-2; $Cr_2(tfa)_4[(EtO)_3PO]_2$, 113274-02-5; $Cr_2(tfa)_4(HMPA)$, 113274-03-6; $Cr_2(tfa)_4(DMTF)(Et_2O)$, 113274-04-7; $Cr_2(tfa)_4(DMCA)(Et_2O)$, 113274-05-8; $Cr_2(tfa)_4(DMF)(Et_2O)$, 113274-06-9; $Cr_2(tfa)_4[(MeO)_3P](Et_2O)$, 113274-07-0; $Cr_2(tfa)_4[(EtO)_3PO](Et_2O)$, 113274-08-1; $Cr_2(tfa)_4(DMA)(Et_2O)$, 113274-09-2; $Cr_2(tfa)_4(DMSO)(Et_2O)$, 113274-10-5; $Cr_2(tfa)_4(Me_3PO)(Et_2O)$, 113274-11-6; $Cr_2(tfa)_4(HMPA)(Et_2O)$, 113274-12-7; $Cr_2(tfa)_4(DMTF)_2$, 113274-13-8; $Cr_2(tfa)_4(DMCA)_2$, 113274-14-9; $Cr_2(tfa)_4(DMF)_2$, 113274-15-0; $Cr_2(tfa)_4[(MeO)_3P]_2$, 113301-74-9; $Cr_2(tfa)_4(Me_4Urea)_2$, 113274-16-1; $Cr_2(tfa)_4(DMA)_2$, 113274-17-2; $Cr_2(tfa)_4(DMSO)_2$, 113274-18-3; $Cr_2(tfa)_4(Me_3PO)_2$, 113274-19-4.

Supplementary Material Available: Tables of molar magnetic susceptibility corrected for diamagnetism with Pascal's constants and raw calorimetry data (15 pages). Ordering information is given on any current masthead page.

Contribution from the Department of Chemistry, Texas A&M University, College Station, Texas 77843

Effect of d-Orbital Occupation on the Coordination Geometry of Metal Hydrates: Full-Gradient ab Initio Calculations on Metal Ion Monohydrates

Randall D. Davy and Michael B. Hall*

Received August 20, 1987

Hartree–Fock–Roothaan self-consistent-field calculations were performed on monohydrates of the metal ions Li^+, Na^+, K^+, Ca^{2+}, Sc^{3+}, Ti^{2+}, Cr^{2+}, Co^+, and Ni^{2+} and the neutral Fe^0. Optimal geometries were calculated with the requirement that *Cs* symmetry be maintained. From these calculations the effect of the electronic interaction on the metal–water coordination geometry was isolated from bulk effects and its strength estimated. Potential energy curves were calculated for the metal ion versus the angle θ_W (the "wag angle"). The potential energy curve for this wagging motion was found to be shallow, and in all cases except Fe^0 the planar, C_{2v}, geometry ($\theta_W = 0°$) was found to have the lowest energy. The potential curve depended strongly on the charge of the ion and weakly on the d-orbital occupation of the transition metals.

Introduction

Metal ion hydration, especially hydration of biologically important alkali metals, has been thoroughly studied and reviewed.[1-3] Clementi and co-workers performed extensive ab initio calculations on alkali-metal ions, including construction of potential energy surfaces for a water molecule in the field of Li^+, Na^+, or K^+ ions.[4,5] They obtained the lowest energy when the metal lies along the water dipole, as in Figure 1 with $\theta_W = 0°$. Dacre did a more detailed study of the Na^+–OH_2 complex and obtained results similar to those of Clementi.[6] The potential energy surface calculated by Clementi for the H_2O–Li^+ complex was subsequently used by Impey et al. in a Monte Carlo simulation.[7] Bounds has used an analytical gradient technique to provide the potential terms for Monte Carlo simulations of dilute aqueous Li^+, Na^+, K^+, Ca^{2+}, and Ni^{2+} solutions.[8] This is an efficient method of calculating a potential energy surface, and earlier Bounds found that a gradient calculation produced a potential surface for Na^+, Li^+, and K^+ in good agreement with that of Clementi.[9]

Although the potential energy surfaces used in the Monte Carlo calculations give minima for θ_W of 0°, the Monte Carlo calculations of Bounds show the tendency of the water to coordinate the metal with θ_W greater than zero, generally 25–45°.[8] This result is in agreement with both crystal structures of metal hydrates[10] and the inelastic neutron scattering experiments of Enderby and co-workers.[11,12] It is postulated that the water–water interactions, especially hydrogen bonding, contribute to θ_W being closer to the tetrahedral value (31.5°) than the planar.

There are still unanswered questions concerning the interaction of water molecules coordinated to metal ions. Calculations on H_3O^+ give a nonplanar geometry for the gas-phase ion. What is the difference between Li^+ and H^+, which makes the former planar and the latter pyramidal? The predominant interaction at a long M–O distance is certainly the ion–dipole interaction, which will favor the planar geometry. At shorter M–O distances, however, one might expect orbital interactions to induce a nonplanar geometry.[13] Enderby's study included the transition-metal ion Ni^{2+}, which has an unfilled d shell. One might therefore ask whether certain d-orbital occupations favor a nonplanar geometry apart from bulk interactions. The transition-metal hydrates have not been studied as extensively as those of the alkali metals, although their hydration geometries are important for understanding reactions such as the electron transfer between $Fe^{II}(H_2O)_6$ and $Fe^{III}(H_2O)_6$.[14] We have attempted to answer these questions by calculating optimal geometries of the hydrates of the spherical ions Li^+, Na^+, K^+, Ca^{2+}, and Sc^{3+}, of the ions Ti^{2+} and Cr^{2+}, with two and four d electrons, and of the ions Fe^0, Co^+, and Ni^{2+}, with eight d electrons. In this study, rather than trying to understand all the interactions in a cluster, we will focus on the effect of the electronic interactions on the coordination geometry of a single

(1) Conway, B. E. *Ionic Hydration in Chemistry and Biophysics*; Elsevier: New York, 1982.
(2) Schuster, P.; Jakubetz, W.; Marius, W. *Top. Curr. Chem.* **1975**, *60*, 1.
(3) Hunt, J. P.; Friedman, H. L. *Adv. Inorg. Chem.* **1983**, *30*, 359.
(4) Clementi, E.; Popkie, H. *J. Chem. Phys.* **1972**, *57*, 1077.
(5) Kistenmacher, H.; Popkie, H.; Clementi, E. *J. Chem. Phys.* **1973**, *58*, 1689.
(6) Dacre, P. D. *Mol. Phys.* **1984**, *51*, 633.
(7) Impey, R. W.; Madden, P. A.; McDonald, I. R. *J. Phys. Chem.* **1983**, *87*, 5071.
(8) Bounds, D. G. *Mol. Phys.* **1985**, *54*, 1335.
(9) Bounds, D. G.; Bounds, P. J. *Mol. Phys.* **1983**, *50*, 25.
(10) Friedman, H. L.; Lewis, L. *J. Solution Chem.* **1976**, *5*, 445.
(11) Enderby, J. E.; Neilson, G. W. *Rep. Prog. Phys.* **1981**, *44*, 38.
(12) Enderby, J. E. *Annu. Rev. Phys. Chem.* **1983**, *34*, 155.
(13) Albright, T. A.; Burdett, J. K.; Whangbo, M. H. *Orbital Interactions in Chemistry*; Wiley-Interscience: New York, 1985; p 106.
(14) (a) Jafri, J. A.; Logan, J.; Newton, M. D. *Isr. J. Chem.* **1980**, *19*, 340. (b) Newton, M. D. *J. Phys. Chem.* **1986**, *90*, 3734. (c) Newton, M. D.; Sutin, N. *Annu. Rev. Phys. Chem.* **1984**, *35*, 437.

0020-1669/88/1327-1417$01.50/0